crystals

MDPI

Article

# Structure and Properties of Cubic $PuH_2$ and $PuH_3$: A Density Functional Theory Study

**Thomas Smith [1], Samuel Moxon [1], David J. Cooke [1], Lisa J. Gillie [1], Robert M. Harker [2], Mark T. Storr [2], Estelina Lora da Silva [3] and Marco Molinari [1,*]**

[1] Department of Chemical Sciences, University of Huddersfield, Queensgate, Huddersfield HD1 3DH, UK
[2] AWE Aldermaston, Reading RG7 4PR, UK
[3] IFIMUP, Department of Physics and Astronomy, Faculty of Science, University of Porto, Rua do Campo Alegre 687, 6169-007 Porto, Portugal
* Correspondence: m.molinari@hud.ac.uk

**Abstract:** The presence of cubic $PuH_2$ and $PuH_3$, the products of hydrogen corrosion of Pu, during long-term storage is of concern because of the materials' pyrophoricity and ability to catalyse the oxidation reaction of Pu to form $PuO_2$. Here, we modelled cubic $PuH_2$ and $PuH_3$ using Density Functional Theory (DFT) and assessed the performance of the PBEsol+$U$+SOC ($0 \leq U \leq 7$ eV) including van der Waals dispersion using the Grimme D3 method and the hybrid HSE06sol+SOC. We investigated the structural, magnetic and electronic properties of the cubic hydride phases. We considered spin–orbit coupling (SOC) and non-collinear magnetism to study ferromagnetic (FM), longitudinal and transverse antiferromagnetic (AFM) orders aligned in the <100>, <110> and <111> directions. The hybrid DFT confirmed that FM orders in the <110> and <111> directions were the most stable for cubic $PuH_2$ and $PuH_3$, respectively. For the standard DFT, the most stable magnetic order is dependent on the value of $U$ used, with transitions in the magnetic order at higher $U$ values ($U > 5$ eV) seen for both $PuH_2$ and $PuH_3$.

**Keywords:** plutonium hydrides; structural properties; magnetic properties; electronic properties; hybrid density functional theory



**Citation:** Smith, T.; Moxon, S.; Cooke, D.J.; Gillie, L.J.; Harker, R.M.; Storr, M.T.; da Silva, E.L.; Molinari, M. Structure and Properties of Cubic $PuH_2$ and $PuH_3$: A Density Functional Theory Study. *Crystals* **2022**, *12*, 1499. https://doi.org/10.3390/cryst12101499

Academic Editor: Francesco Stellato

Received: 5 October 2022
Accepted: 19 October 2022
Published: 21 October 2022



## 1. Introduction

The UK has a long history of nuclear power generation dating from the opening of Calder Hall reactor at Sellafield in 1956 [1], with a range of reactor types generating plutonium as a by-product of the power generation [2,3]. Throughout this history, the dominant plutonium material type for both research and use has been the dioxide, $PuO_2$: its chemical stability makes it useful as a fuel and for storage.

Plutonium hydrides are less studied in comparison [4] but are nevertheless an important class of compounds. Firstly, metallic plutonium corrodes in the presence of hydrogen or water (gas or liquid) to form hydrides and hydride containing mixtures, and similar products are formed if plutonium metallic materials are held in close proximity to hydrogenous materials (polymers, oils, etc.), which can radiolytically decay and generate hydrogen. The hydrides formed in such scenarios are often friable, high surface area materials that react vigorously with air, presenting a pyrophoric hazard [5]. Additionally, the volume increase associated with formation of hydrides could theoretically lead to mechanical strain on storage containers [6–8]. Thus, waste packages that might contain plutonium metallic materials could present specific hazards if they are generating hydrides during long periods of storage: the subsequent opening in a controlled or uncontrolled fashion in an air environment could ignite plutonium hydride materials. Secondly, plutonium hydrides are a component of mixed hydride fuels such as PUZH ($PuH_2$-U-$ZrH_{1.6}$) that are reported to have a higher burnup opportunity (103 vs. 50 GWD/MTiHM for mixed oxide fuels (MOX)) [9]. In addition, a PUZH core is estimated to cost ~13% less than a MOX core,

and to be superior to mixed oxide fuels MOX in terms of transmutation effectiveness and proliferation resistance [10].

There are two accepted phase diagrams for the Pu+H system. Firstly, that of Wicke [11] and of Flotow [12] and secondly that of Haschke et al. [5] The earlier work implies that the $PuH_{2+x}$ cubic form is present from $PuH_2$ to $PuH_3$ although is non-committal at high temperatures. Alternatively, the Haschke phase diagram indicates that increasing complexity creeps in above $PuH_{2.7}$ with first a mixed phase region (cubic + hexagonal), then hexagonal and then orthorhombic (an unidentified further phase is also suggested in this phase range). These two-phase diagrams are not necessarily in disagreement and Haschke himself notes that the discrepancy is probably due to preparation methods (the cubic form would appear to be observed above $PuH_{2.7}$ if the hydride is prepared at higher temperatures). So, to summarise the literature consensus that the cubic form of $PuH_x$ is observed between $PuH_{1.95}$ and $PuH_{2.7}$ and the cubic form may or may not be found at higher hydrogen stoichiometries depend on the preparation conditions. In $PuH_2$, hydrogen occupies the tetrahedral sites ($H_T$), and the additional hydrogen in a $PuH_3$ cubic structure is accommodated within the octahedral sites ($H_O$) (Figure 1). A large activation energy prevents the cubic to hexagonal phase transition at lower temperatures [5,13].

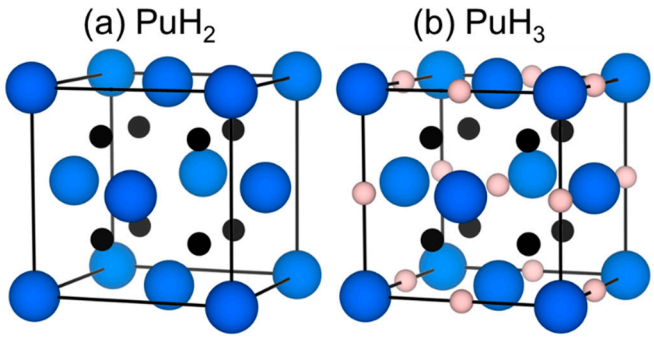


**Figure 1.** Crystal structures of cubic (**a**) $PuH_2$ and (**b**) $PuH_3$. Pu in blue and H occupying tetrahedral sites ($H_T$) in black and octahedral sites ($H_O$) in pink.

Experimental studies on Pu materials are challenging due to the toxic and radioactive nature of the materials [14,15]. Computational studies, utilising first principles techniques, have been employed with different levels of complexity, for instance using DFT including on-site Coulombic correction Hubbard parameter $U$ [16–26], spin–orbit coupling (SOC) [18,20,21,24–27], and hybrid [28] functionals. Theoretical studies have shown the ability to produce accurate descriptions of the properties of cubic $PuH_2$ and $PuH_3$. For example, the lattice contraction that occurs in $PuH_x$ as x increases from x = 2 to 3 [17,21,26,28] agreeing with experimental X-ray diffraction (XRD) [29] data, and the metal-insulator transition (MIT) [21,27] agreeing with a DC experiment [30].

In this study, we model cubic $PuH_2$ and $PuH_3$ using Density Functional Theory (DFT) using two levels of theory PBEsol+$U$+SOC ($0 \leq U \leq 7$ eV) and hybrid HSE06sol+SOC, including spin orbit coupling (SOC) and non-collinear magnetism, to investigate their structure, and magnetic and electronic properties. In particular, the order of stability of ferromagnetic (FM), longitudinal antiferromagnetic (AFM) and transverse AFM orders in the <100>, <110>, and <111> directions.

## 2. Computational Methodology

$PuH_x$ was investigated using a non-collinear relativistic computational method employing DFT within the Vienna Ab initio Simulation Package (VASP) [31]. Our simulations use a plane-wave basis set incorporating relativistic core potentials and ion-electron interactions described using the project augmented wave (PAW) method [32]. The inclusion of spin–orbit coupling (SOC) [33] is deemed important in the previous literature [26], thus is included in this study. We applied the generalised gradient approximation (GGA) with

the Perdew–Burke–Ernzerhof for solids (PBEsol) [34] functional and the hybrid functional of Heyd–Scuseria–Ernzerhof for solids (HSE06sol) [35]. To describe the strong on-site Columbic repulsion of Pu 5f electrons using the PBEsol functional, the Hubbard $U$ correction was applied. In the Liechtenstein method [36], the Coulombic ($U$) and the exchange ($J$) parameters are treated as independent variables. We evaluated values of $U$ between 0 and 7 eV with $J$ = 0 eV, and hence this method becomes equivalent to the Dudarev method [37]. The effective $U$ parameter, $U_{\text{eff}} = U - J$, is referred to as $U$ from now on. Following convergence testing, see Table S1, the cut-off energy for the planewave basis set is 1000 eV (PBEsol+$U$+SOC) and 500 eV (HSE06sol+SOC). The Brillouin zone was sampled using a ***k***-point grid of 11 × 11 × 11 for PBEsol+$U$+SOC for both the calculations for the geometry optimisation and the electronic density of states, and 5 × 5 × 5 for HSE06sol+SOC calculations. The electronic and ionic iteration convergence criteria for the bulk structures of cubic $PuH_2$ and $PuH_3$ were $1 \times 10^{-5}$ eV per atom and $1 \times 10^{-3}$ eV Å$^{-1}$, respectively. A total of nine magnetic orders were considered, consisting of ferromagnetic, longitudinal antiferromagnetic and transverse antiferromagnetic orders in the <100>, <110> and <111> alignments. The non-collinear magnetic wave vectors are as shown in Figure 2. The terminology 1k, 2k and 3k refers to the alignment of the magnetic moments in the <100>, <110> and <111> directions, respectively, and is common terminology when it comes to $UO_2$, $NpO_2$ and $PuO_2$ [38–40].

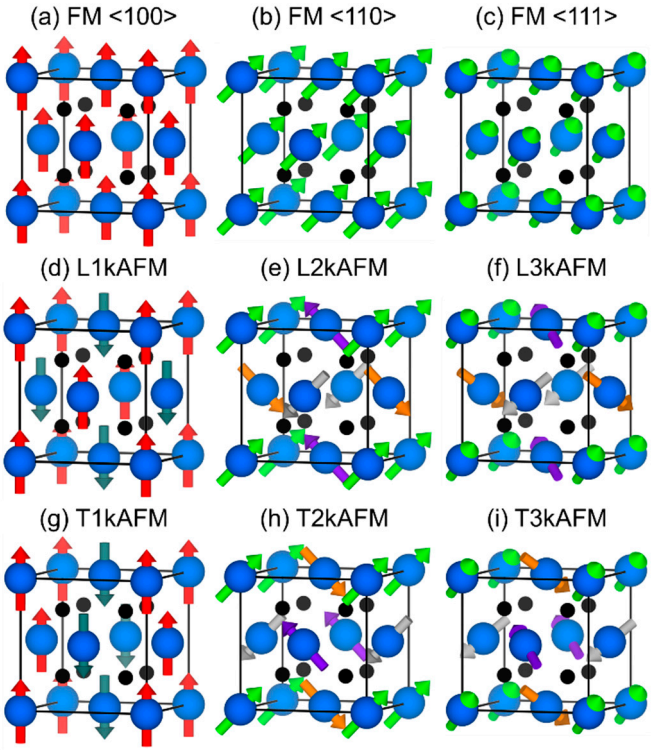


**Figure 2.** Magnetic structure of cubic $PuH_x$ with FM (**a**) <100>, (**b**) <110>, (**c**) <111>, longitudinal AFM (**d**) 1k, (**e**) 2k, (**f**) 3k, and transverse AFM (**g**) 1k, (**h**) 2k and (**i**) 3k. Pu in blue and H occupying tetrahedral sites ($H_T$) in black for $PuH_2$. The presence of H occupying octahedral sites ($H_O$) in $PuH_3$ would not change the directions of the magnetisation on Pu atoms.

## 3. Results and Discussion

The most stable magnetic order amongst ferromagnetic <100>, <110> and <111>, longitudinal antiferromagnetic 1k, 2k and 3k, and transverse antiferromagnetic 1k, 2k and 3k orders, which we will refer to as FM <100>, FM <110>, FM <111>, L1kAFM, L2kAFM, L3kAFM, T1kAFM, T2kAFM and T3kAFM, respectively, was determined using HSE06sol+SOC and PBEsol+$U$+SOC ($0 \leq U \leq 7$ eV) functionals considering non-collinear

magnetic contributions. The advantage of computational techniques is that they allow one to simulate different structural models and impose structural constraints to evaluate whether they are or could be stable. For example, a small distortion of the oxygen sublattice has been reported in fluorite $UO_2$, which caused a lowering of symmetry from $Fm\bar{3}m$ to $Pa\bar{3}$ [40,41]. We have also applied such distortion on the hydrogen sublattice in both cubic $PuH_2$ and $PuH_3$. However, all our attempts to geometry optimise these structures removed the distortion in the hydrogen sublattice for all magnetic orders and for all values of the Hubbard $U$ parameter used ($0 \leq U \leq 7$ eV). We have also studied the inclusion of van der Waals (vdW) dispersions using the D3 method of Grimme et al. [42] (PBEsol+$U$+SOC+D3) considering non-collinear magnetic contributions. Our results using vdW corrections are consistent to those without vdW in terms of energy differences (Table S2), magnetism (Table S3), symmetry (Table S4), and lattice parameters for $PuH_2$ (Table S5) and $PuH_3$ (Table S6) and their average values (Figure S1), thus PBEsol+$U$+SOC+D3 results are presented in the SI.

### 3.1. Thermodynamic Stability

The relative energetics of cubic $PuH_2$ and $PuH_3$ calculated using HSE06sol+SOC are reported in Figure 3.

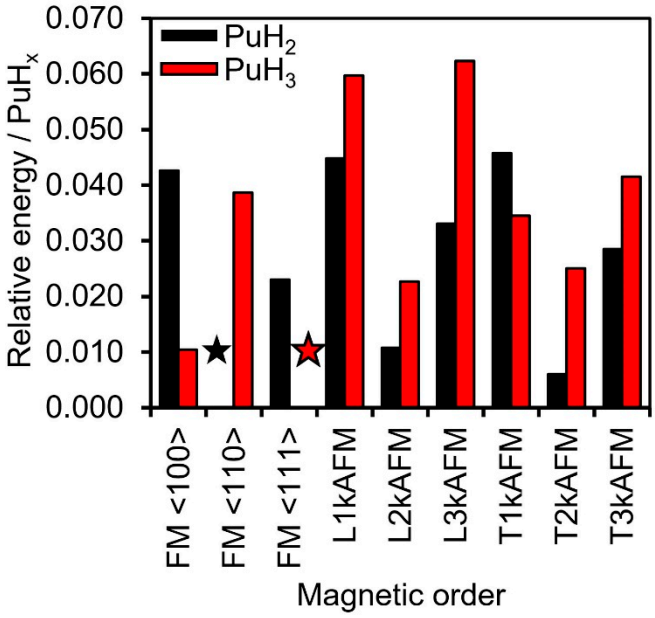


**Figure 3.** Relative energies of FM <100>, <110> and <111>, longitudinal AFM 1k, 2k and 3k, and transverse AFM 1k, 2k and 3k magnetic orders per $PuH_x$ for $PuH_2$ in black and for $PuH_3$ in red, calculated using HSE06sol+SOC. Black and red stars represent the most stable magnetic order for $PuH_2$ and $PuH_3$, respectively.

For both structures, our data indicates that the FM order is the most stable. For $PuH_2$, the most stable alignment is in the <110> direction followed by <111> and then <100> for each of the three magnetisms, i.e. FM, longitudinal AFM, and transverse AFM. The most stable magnetic order overall for $PuH_2$ is FM <110>; however only a very small difference ($6.0 \times 10^{-3}$ eV/$PuH_2$) is predicted to the next most stable order T2kAFM. For $PuH_3$, alignment in the <111> direction is most stable for FM orders, followed by <100> and <110> directions. For longitudinal and transverse AFM orders, the alignment in the <110> direction is most stable followed by the ones in the <100> and <111> directions. The most stable magnetic order overall is FM <111>; however only a $1.0 \times 10^{-2}$ eV/$PuH_3$ difference is predicted to the next most stable order FM <100>. Such small differences in relative energy are mostly of the order of $k_bT$ at room temperatures, i.e., $2.6 \times 10^{-2}$ eV, suggesting that magnetic orders could co-exist. This is supported by both experimental [30,43] and

computational [21,26,28] investigations where either FM and AFM orders are predicted as most stable for $PuH_2$, and only very small energy differences exist between both orders for $PuH_2$ and $PuH_3$.

Experimentally, using a vibrating sample magnetometer (VSM), Willis et al. [30] ($PuH_x$ with x = 1.93, 45 K) and Kim et al. [44] ($PuH_x$ with x = 1.9, 40 K) found the FM order to be the most stable. Whilst, the AFM order was also experimentally determined as most stable for $PuH_2$ by Aldred et al. [43] ($PuH_x$ with x = 1.99, 30 K) using the Faraday method in agreement with the nuclear magnetic resonance (NMR) results of Cinader et al. [45] Such a difference in magnetic order obtained by the experiments was attributed to differences in samples and compositions by Willis et al. [30] However, the determination of the correct composition and magnetic properties of $PuH_x$ is difficult to obtain experimentally as thermodynamic equilibrium has to be reached, in addition to a possible oxidation of the sample, i.e., where the fluorite $PuO_2$ structure may also be present as a surface layer onto the Pu metal [43].

Computationally, the hybrid PBE0 (without SOC) of Li et al. [28] found that the FM <100> order is more stable than the 1k AFM order for both cubic $PuH_2$ and $PuH_3$ with only small energy differences, i.e., $E_{FM}$-$E_{AFM}$ of $-5.4 \times 10^{-2}$ eV for $PuH_2$ and $-4.1 \times 10^{-2}$ eV for $PuH_3$. For $PuH_2$, using HSE06sol+SOC we found the order of stability in the <100> alignment is FM <100> > L1kAFM > T1kAFM, which agrees with findings from an alternative hybrid method of Li et al. [28]. The energy differences we predict between orders are very small with only $-2.2 \times 10^{-3}$ eV between FM <100> and L1kAFM, and $-3.1 \times 10^{-3}$ eV between FM <100> and T1kAFM. For $PuH_3$, using HSE06sol+SOC we found that the order of stability in the <100> direction is FM <100> > T1kAFM > L1kAFM, with small energy differences of $-2.4 \times 10^{-2}$ eV between FM <100> and T1kAFM, and $-4.9 \times 10^{-2}$ eV between FM <100> and L1kAFM. Furthermore, the GGA+$U$+SOC study of Guo et al. [21] found FM to be more stable than AFM for both $PuH_2$ and $PuH_3$, agreeing with the present work and Li et al. [28] Although the alignment of the magnetic order is not specified, small differences in energy are reported, i.e. $E_{FM}$-$E_{AFM}$ was only $-2.7 \times 10^{-3}$ eV for $PuH_2$ and $-2.7 \times 10^{-2}$ eV for $PuH_3$, respectively [21]. The AFM order was found to be more stable than FM using LDA(GGA)+$U$ (unstated alignment) for cubic $PuH_2$ and $PuH_3$ [26] and using PBE+$U$ (spin magnetic moments aligned in a simple "up down up down" alternative manner along the <111> direction, $U$ = 3.25 eV) for $PuH_2$ [46]. A transition is observed in the magnetic order of $PuH_2$ from AFM to FM when $U$ = 4 eV for LDA+$U$ and from FM to AFM when $U$ = 1 eV for GGA+$U$. The introduction of SOC was deemed important, with FM state predicted as more stable for $PuH_3$; however, the AFM order was still most stable for $PuH_2$ [26].

We calculate only very small differences in relative energies amongst all the magnetic orders for each value of the Hubbard $U$ using PBEsol+$U$+SOC for both cubic $PuH_2$ and $PuH_3$ (Figure 4). We find a transition between the most stable magnetic orders in both $PuH_2$ and $PuH_3$, which is dependent on the value of $U$ used.

For $PuH_2$, and considering PBEsol+$U$+SOC when $0 \leq U \leq 4$ eV, T2kAFM is the most stable magnetic order but when $5 \leq U \leq 7$ eV FM <110> order is the most stable, implying that a transition occurs at $U$ = 5 eV from AFM to FM, which is comparable to that obtained by Zheng et al. [26] at $U$ = 4 eV using LDA+$U$. When comparing with our results from HSE06sol+SOC, FM <110> and T2kAFM are the most stable and next most stable orders, displaying how sensitive the magnetism is upon the choice of the Hubbard correction.

As for $PuH_3$, only a very small difference in energy ($6.2 \times 10^{-2}$ eV) was predicted between the most stable magnetic order FM <111> and the least stable L3kAFM using HSE06sol+SOC. By employing PBEsol+$U$+SOC, the relative energies display a more complicated behaviour for $PuH_3$. There is a transition in stability between the FM and AFM order at $U$ = 6 eV. However, when $U$ = 0 eV, $U$ = 1 eV, $2 \leq U \leq 5$ eV the most stable orders are FM <100>, FM <110>, and FM <111>, respectively, whereas when $6 \leq U \leq 7$ eV the most stable order is T2kAFM.

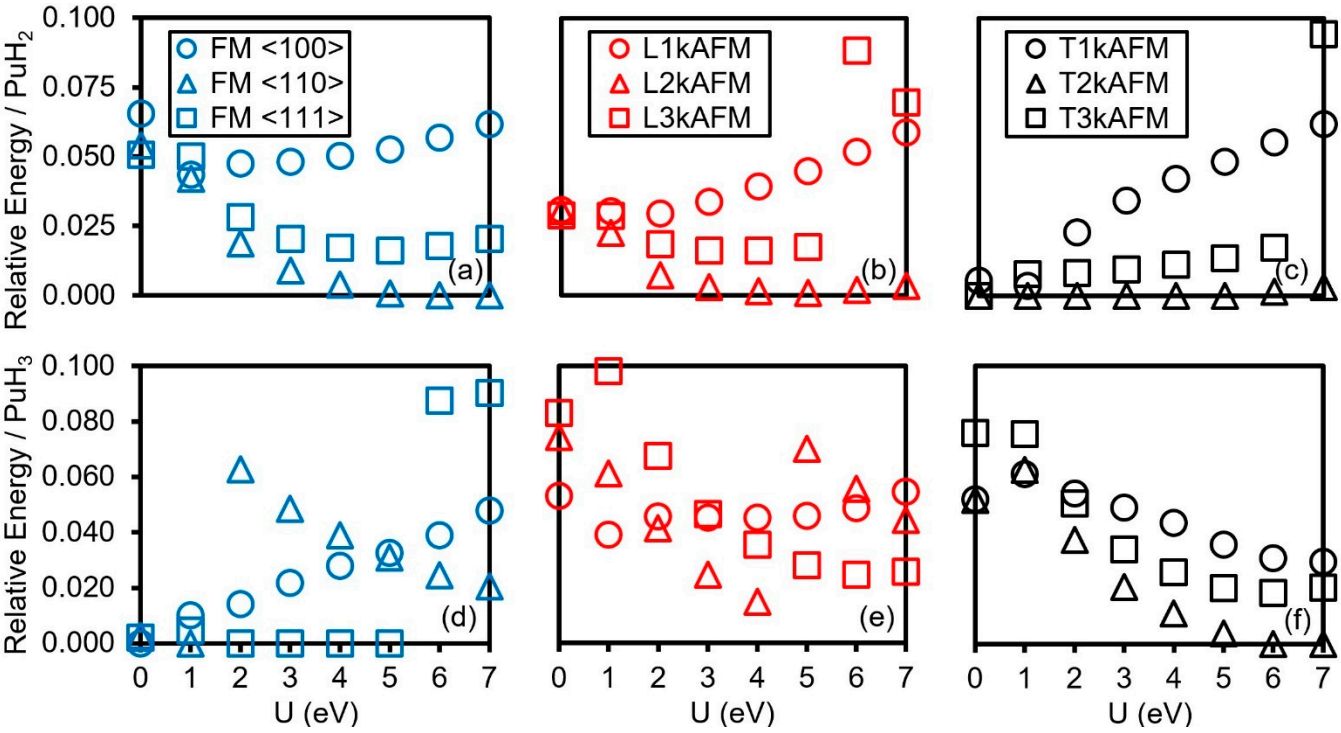


**Figure 4.** Relative energies per formula unit for cubic $PuH_2$ (**a**) FM <100>, <110>, <111>, (**b**) longitudinal AFM 1k, 2k and 3k, and (**c**) transverse AFM 1k, 2k and 3k, and for $PuH_3$ (**d**) FM <100>, <110> and <111>, (**e**) longitudinal AFM 1k, 2k and 3k, and (**f**) transverse AFM 1k, 2k and 3k calculated with PBEsol+$U$+SOC ($0 \leq U \leq 7$ eV).

Instabilities in the energy trends of $PuH_2$ where found, for example in L3kAFM at $U$ = 6 and T3kAFM at $U$ = 7 which do not follow the trend. This may be due to the DFT+$U$ methodology, which has issues in stabilising metastable states as the degeneracy of the f orbitals is broken. The energy minimisation that optimised the geometry may thus lead the system to be "trapped" in a metastable state. There are methodologies, such as occupation matrix control (OMC) [47] and $U$-ramping [48] that can help with the DFT+$U$ localisation issues to reach the ground state. Applying DFT+$U$+OMC would require the consideration of all possible initial occupation matrices, making the method time consuming and complicated for a system such as cubic $PuH_x$ with a high number of electronic configurations. On the other hand, by choosing the $U$-ramping method, one has to consider that it can only be applied when the selected $U$ value does not change the orbital ordering. We tested $U$-ramping on selected structures and yet could not eliminate the instabilities in the energy trend.

### *3.2. Symmetry and Structure*

Space groups of the optimised cubic $PuH_2$ and $PuH_3$ phases using FM and AFM magnetic orders are shown in Table 1 for both HSE06sol+SOC and PBEsol+$U$+SOC calculations. Only the L3kAFM order maintained the cubic experimentally derived $Fm\bar{3}m$ symmetry for both $PuH_2$ and $PuH_3$. Supported by both our hybrid and standard DFT calculations, the space group symmetry of $PuH_2$ and $PuH_3$ are the same but display a lowering of symmetry with a distortion on one of the three lattice parameters (see Tables S8 and S9 for full details).

**Table 1.** Space groups calculated with HSE06sol+SOC and PBEsol+$U$+SOC with a tolerance of $10^{-5}$ Å for FM <100>, <110> and <111>, longitudinal and transverse AFM 1k, 2k and 3k order for cubic $PuH_2$. For cubic $PuH_3$, the space groups are the same apart from the ones in brackets, which refers to the space group for $PuH_3$ when it differs from that of $PuH_2$. Space group numbers: $I4/mmm$ (139), $P\bar{1}$ (2), $C2/m$ (12), $Immm$ (71), $R\bar{3}m$ (166), $Fm\bar{3}m$ (225), $Fmmm$ (69), $Cmca$ (64), $Pbca$ (61) and $Pa\bar{3}$ (205).

| Magnetic Order | PBEsol+$U$+SOC—$U$ (eV) | | | | | | | | HSE06sol +SOC |
|---|---|---|---|---|---|---|---|---|---|
| | 0 | 1 | 2 | 3 | 4 | 5 | 6 | 7 | |
| FM <100> | $I4/mmm$ | $I4/mmm$ | $I4/mmm$ | $I4/mmm$ | $I4/mmm$ | $I4/mmm$ | $I4/mmm$ | $I4/mmm$ | $I4/mmm$ |
| FM <110> | $P\bar{1}$ | $C2/m$ | $C2/m$ | $C2/m$ | $C2/m$ | $C2/m$ | $C2/m$ | $C2/m$ | $Immm$ ($C2/m$) |
| FM <111> | $R\bar{3}m$ | $R\bar{3}m$ | $R\bar{3}m$ | $R\bar{3}m$ | $R\bar{3}m$ | $R\bar{3}m$ | $R\bar{3}m$ | $R\bar{3}m$ | $R\bar{3}m$ |
| L1kAFM | $I4/mmm$ | $I4/mmm$ | $I4/mmm$ | $I4/mmm$ | $I4/mmm$ | $I4/mmm$ | $I4/mmm$ | $I4/mmm$ | $I4/mmm$ |
| L2kAFM | $I4/mmm$ | $I4/mmm$ | $I4/mmm$ | $I4/mmm$ | $I4/mmm$ | $I4/mmm$ | $I4/mmm$ | $I4/mmm$ | $I4/mmm$ |
| L3kAFM | $Fm\bar{3}m$ | $Fm\bar{3}m$ | $Fm\bar{3}m$ | $Fm\bar{3}m$ | $Fm\bar{3}m$ | $Fm\bar{3}m$ | $Fm\bar{3}m$ | $Fm\bar{3}m$ | $Fm\bar{3}m$ |
| T1kAFM | $Fmmm$ | $Fmmm$ | $Fmmm$ | $Fmmm$ | $Fmmm$ | $Fmmm$ | $Fmmm$ | $Fmmm$ | $Fmmm$ |
| T2kAFM | $Cmca$ | $Cmca$ | $Cmca$ ($Pbca$) | $Cmca$ | $Cmca$ | $Cmca$ | $Cmca$ | $Cmca$ | $Pbca$ ($Fmmm$) |
| T3kAFM | $Pa\bar{3}$ | $Pa\bar{3}$ | $Pa\bar{3}$ | $Pa\bar{3}$ | $Pa\bar{3}$ | $Pa\bar{3}$ | $Pa\bar{3}$ | $Pa\bar{3}$ | $Pa\bar{3}$ |

Good agreement is found between HSE06sol+SOC and PBEsol+$U$+SOC with the same symmetry predicted for all phases apart from a small difference in FM <110> and T2kAFM orders. Between $PuH_2$ and $PuH_3$ the same symmetry is determined, except for HSE06sol+SOC FM <110> and T2kAFM and PBEsol+$U$+SOC T2kAFM where $U$ = 2 eV. Using HSE06sol+SOC, the cell lengths for the most stable magnetic order of $PuH_2$ (FM <110>) are a = b = 5.33 Å and c = 5.28 Å, and for the most stable magnetic order of $PuH_3$ (FM <111>) is 5.24 Å. Only a difference of 0.59% was calculated between the hybrid value obtained for the lattice parameters of cubic $PuH_2$ and the experimental value of Mulford et al. [49,50] (5.359 Å). For cubic $PuH_3$, a 1.97% difference in the lattice parameters was determined compared to the experimental value of Muromura et al. [29] (5.34 Å).

In Figure 5 the average cell length and angles for each magnetism are plotted as a function of the $U$ value (0–7 eV) for the PBEsol+$U$+SOC calculations, along with the values from HSE06sol+SOC and experiments. The individual values for cell lengths, cell angle and cell volumes are shown in Tables S8 and S9 for $PuH_2$ and $PuH_3$, respectively. At least $U$ = 2–3 eV is required to reproduce the values from the HSE06sol+SOC, but $U$ > 4 eV are the minimum satisfactory values to gain experimental comparison; although this comparison is more accurate for $PuH_2$ (Figure 5a) than for $PuH_3$ since a contraction of the simulated cell at all $U$ values (Figure 5b) is evidenced. A lattice contraction is observed between x = 2 and x = 3, as the ionic character increases with an increase in x, resulting in a lattice contraction due to an increase cell cohesion [16,17,19–21].

Cell lengths for cubic $PuH_2$ with the FM order as 5.454 Å and the AFM order as 5.388 Å, and for $PuH_3$ with FM as 5.35 Å and AFM as 5.35 Å (all magnetic orders where in the [001] direction) were reported by Li et al. [28] using PBE0. For a magnetism aligned in the [001], a distortion in the lattice would be expected in a cubic structure, see the work on $UO_2$, $NpO_2$ and $PuO_2$ [38–40]. Our lattice parameter predicted using HSE06sol+SOC are comparable to those obtained by Li et al. [28]. When comparing our values in the same alignment for each magnetism (i.e., FM <100>, L1kAFM and T1kAFM) we find only small percentage differences of between 0.8 and 3.2% for $PuH_2$ and 0.44–7.82% for $PuH_3$.

As for PBEsol+$U$+SOC ($U$ = 5 eV), the cell length obtained for the L3kAFM magnetic order of cubic $PuH_2$ is 5.36 Å, which agrees perfectly well with the experimental findings of 5.36 Å from Mulford et al. [49,50] for $PuH_2$. L3kAFM was chosen for comparison as it was the only magnetic order to retain $Fm\bar{3}m$ symmetry and $U$ = 5 eV was chosen as cell lengths are accurately described. As the Hubbard $U$ parameter increased from 0 to 7 eV using L3kAFM, a 3.96% increase in cell length is seen; this is due to the 5f electrons becoming more localised leading to a reduction in cohesion energies and an increase in cell length. For cubic $PuH_3$ with the L3kAFM magnetic order using PBEsol+$U$+SOC when $U$ = 5, a cell length of 5.32 Å is in good agreement (0.34% difference) with the experimental finding

of 5.34 Å from Muromura et al. [29] All magnetic orders are in good agreement with the experimental value when $U$ = 5 eV For L3kAFM, a 3.28% increase in cell length is seen when $U$ is increased from 0 to 7 eV.

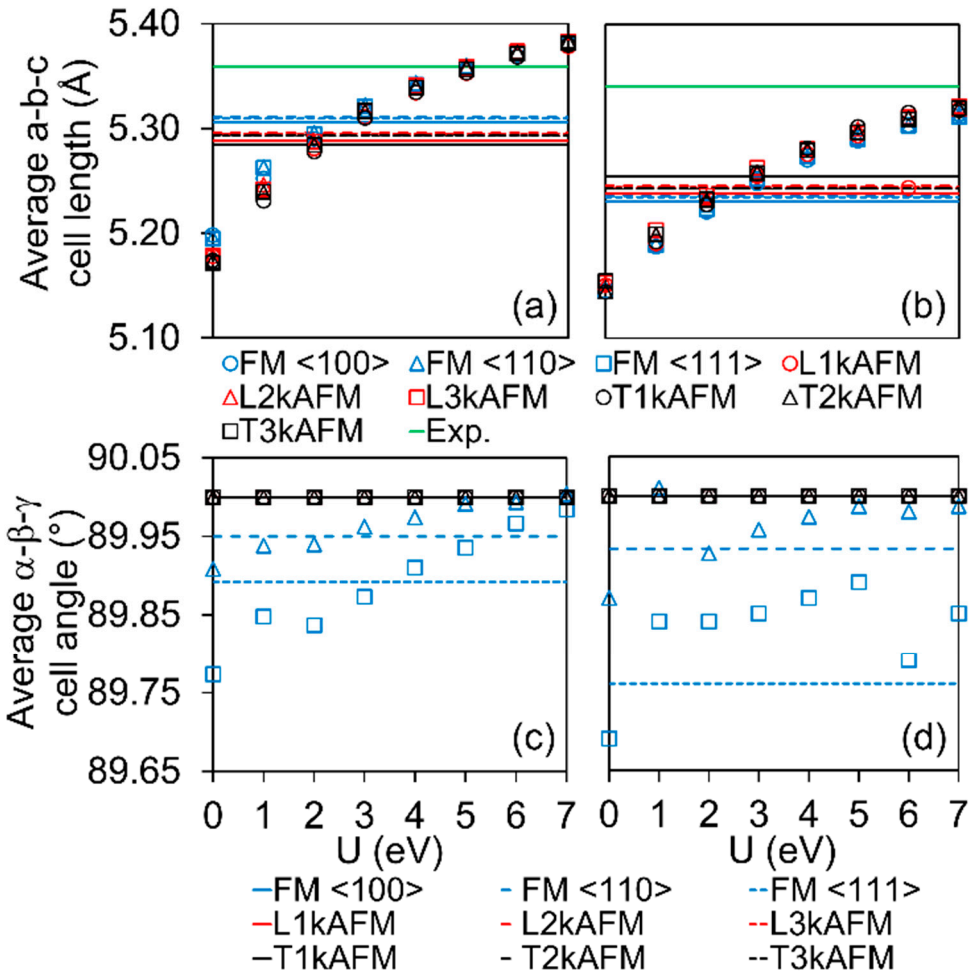


**Figure 5.** Average cell lengths a-b-c (Å) for cubic (**a**) $PuH_2$ and (**b**) $PuH_3$ and average cell angles $\alpha$-$\beta$-$\gamma$ (degree) for (**c**) $PuH_2$ and (**d**) $PuH_3$. Where PBEsol+$U$+SOC ($U$ = 0–7 eV) method is represented by circles, triangles and squares symbols for <100>, <110> and <111> alignments, respectively, and HSE06sol+SOC method is represented by solid, dash and square dotted lines for <100>, <110> and <111>, respectively. FM in blue, LAFM in red, TAFM in black. Experimental cell lengths represented in green for $PuH_2$ (Mulford et al. [49,50]) and $PuH_3$ (Muromura et al. [29]).

### *3.3. Magnetic Moments*

The spin ($\mu_s$), orbital ($\mu_l$) and total ($\mu_{total}$) magnetic moments for cubic $PuH_2$ and $PuH_3$ calculated with HSE06sol+SOC and PBEsol+$U$+SOC are shown in Figure 6. Values of magnetic moments are consistent in magnitude regardless of the magnetic structure imposed on the system when using HSE06sol+SOC. The optimised magnetic wavevectors of $PuH_2$ predicted using HSE06sol+SOC are presented in Table S7. By considering PBEsol+$U$+SOC, the average values for all magnetic orders of $PuH_2$ the total magnetic moments decrease from 2.06 to 1.26 $\mu_B$/atom (38% decrease) when $U$ increased from 0 to 7 eV. For the spin magnetic moment an increase from 4.54 to 4.86 $\mu_B$/atom (7% increase) occurs, whilst for the orbital moment a change from −2.48 to −3.60 $\mu_B$/atom (45% decrease) takes place when $U$ increases from 0 to 7 eV. We find good agreement between hybrid and standard DFT methods.

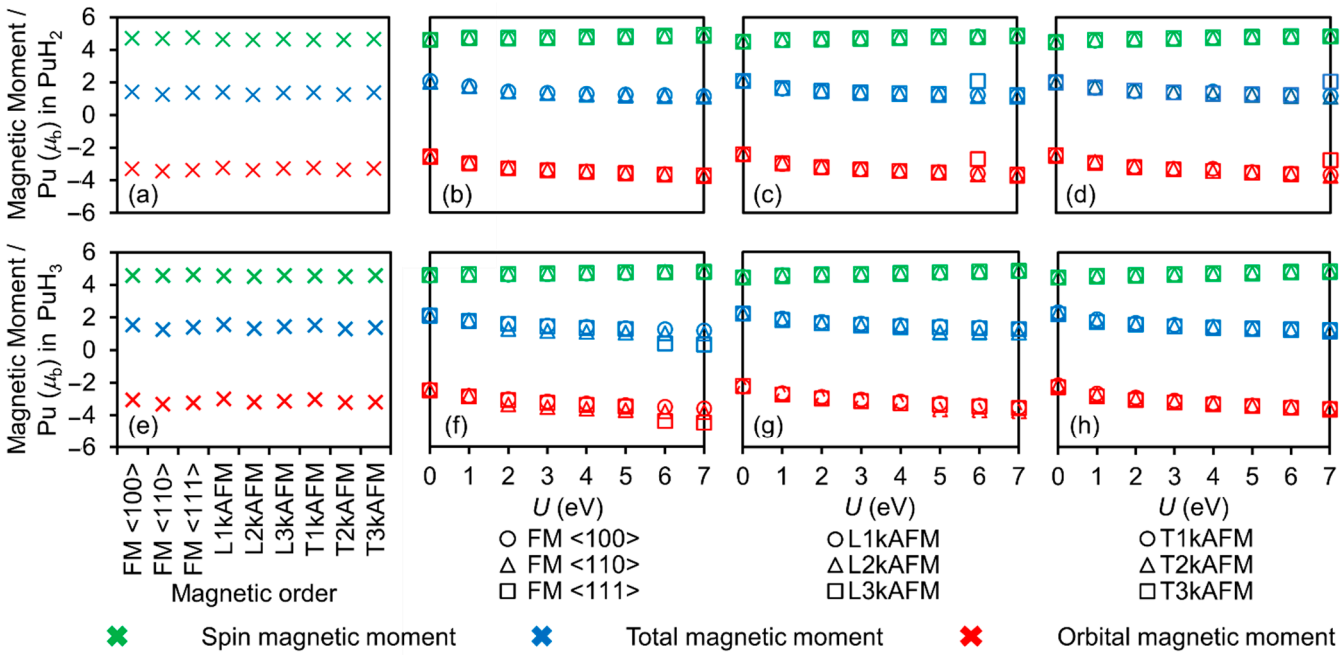


**Figure 6.** Spin (green), orbital (red) and total (blue) magnetic moments calculated using HSE06sol+SOC for (**a**) cubic $PuH_2$ and for (**e**) $PuH_3$ and using PBEsol+$U$+SOC for cubic $PuH_2$ and for $PuH_3$ (**b**,**f**) FM <100>, <110> and <111>, (**c**,**g**) longitudinal AFM 1k, 2k and 3k, and (**d**,**h**) transverse AFM 1k, 2k and 3k.

Spin, orbital, and total magnetic moments were calculated by Zheng et al. [26] using LDA+$U$+SOC ($U$ = 4 eV); which were found to be 4.58, −3.69 and 0.89 $\mu_B$/atom, respectively for $PuH_2$ with an AFM order. These are comparable to the values we obtained for the spin, orbital, and total magnetic moments using PBEsol+$U$+SOC ($U$ = 4 eV) for $PuH_2$ with the T2kAFM order (the most stable for that particular value of $U$) of 4.73, −3.43 and 1.30 $\mu_B$/atom, respectively. All DFT studies overestimate the total magnetic moments in comparison to experimental values for saturated moment of 0.44 $\mu_B$/ion of Aldred et al. [43] for cubic $PuH_{1.99}$, and 0.43 $\mu_B$/ion of Willis et al. [30].

### *3.4. Electronic Structure*

As we compare the performance of the PBEsol+$U$+SOC depending on the value of $U$, the electronic density of states (eDOS) for cubic $PuH_2$ and $PuH_3$ are shown in Figure 7. As the previous session has shown that values of $U$ = 4–6 eV give the best answer in terms of lattice parameters, we have only reported the eDOS for $U$ = 5 eV here. eDOS for $U$ = 4 and 6 eV for both $PuH_2$ and $PuH_3$ can be found in Figures S2 and S3, respectively. Our findings suggest that independent of the value of the $U$ parameter, and of all magnetic orders imposed to the hydrides, cubic $PuH_2$ and $PuH_3$ are both metallic, as there is a non-zero occupancy at the Fermi level, $E_F$. The valence band and conduction band are dominated by Pu 5f states, as is observed in the literature [16,17,20,21]. The non-zero occupancy at the Fermi level in $PuH_3$ is much less pronounced compared to $PuH_2$. The covalent character result from Pu 6d and H 1s hybridisation is observed in the projected DOS for cubic $PuH_x$ (x = 2 and 3) (Figure 7). The on-site Hubbard parameter $U$ increases the localisation of Pu 5f electrons, which separates and sharpens the 5f states [16,17,19–21].

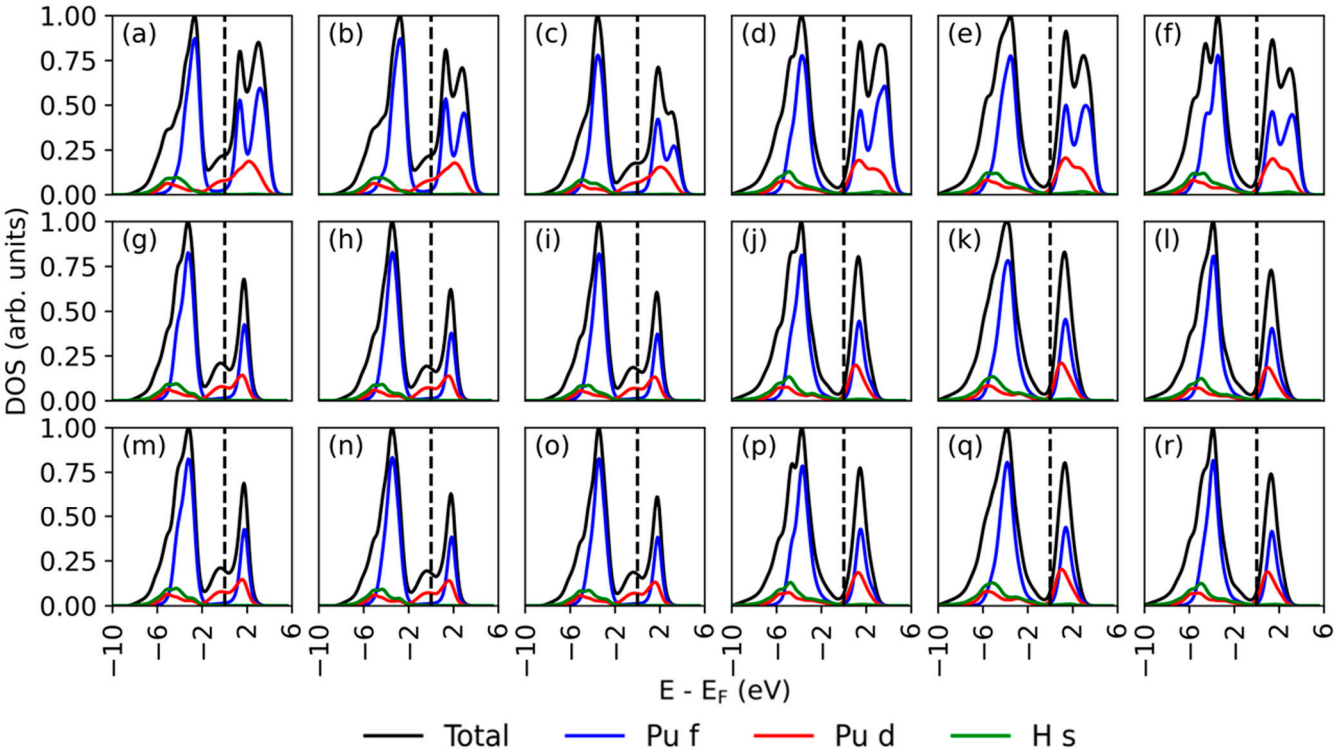


**Figure 7.** eDOS plots calculated using PBEsol+$U$+SOC ($U$ = 5 eV) for cubic $PuH_2$/$PuH_3$ with: FM (**a**,**d**) <100>, (**b**,**e**) <110> and (**c**,**f**) <111>; longitudinal AFM (**g**,**j**) 1k, (**h**,**k**) 2k, and (**i**,**l**) 3k; and transverse AFM (**m**,**p**) 1k, (**n**,**q**) 2k, and (**o**,**r**) 3k. The Fermi level is at 0 eV denoted by a vertical dashed line.

Many computational studies agree with our PBEsol+$U$+SOC results for cubic $PuH_2$, i.e., LDA/LDA+$U$ [16,17,19,26] and GGA/GGA+$U$ [20,21], and for $PuH_3$, i.e., LDA/LDA+$U$ [17,26], GGA/GGA+$U$ [20,21] and PBE+$U$ [22] where it is reported that only a small number of electrons crosses the Fermi level. However, there is also some controversy. The GGA+sp+$U$ ($U$ = 4 eV) of Guo et al. [21] using the full potential linearised augmented plane wave method (FP-LAPW) reports semiconductor behaviour with a bandgap of 0.35 eV for cubic $PuH_3$. If the introduction of SOC changes the nature of the electronic behaviour, we do not see such change in agreement with the LDA+$U$+SOC ($U$ = 4 eV) of Zheng et al. [26]. In addition to the metallic behaviour for cubic $PuH_2$, Li et al. [27] reported semiconductor behaviour also cubic $PuH_3$ at 300K using DFT+$U$ ($U$ = 4.2 eV) and the Dynamical Mean-Field Theory (DMFT). However, somehow their predictions suggest that the occupancy of Pu 5f states would result in $Pu^{3+}$ valence for both $PuH_2$ and $PuH_3$ phases. To note, the Pu 5f electrons are at the boundary between the early actinides with itinerant 5f electrons and the late actinides with localised 5f electrons. Any change in temperature, pressure and chemical potential (i.e., composition) may result in the transition between itinerancy and localisation, causing mixed-valent states or valence fluctuations. This poses issue when simulating $PuH_x$ phases using DFT.

Experimentally, a metal to insulator (MIT) transition was observed by Willis et al. [30] and Ward et al. [51] for cubic $PuH_x$ between x = 1.93 and 2.65. Cubic $PuH_x$ phases were grown on metallic support (Ga doped δ-Pu metal) as described by Haschke et al. [52], but information on sample thickness and support thickness was not reported. Using a four-terminal DC method, a possible transition is recorded at x = 2.14 while a definite transition occurred at x = 2.65 as the rate change in resistivity against temperature becomes negative [30,51].

## 4. Conclusions

Cubic $PuH_2$ and $PuH_3$ were investigated computationally using DFT with two levels of theory: the hybrid HSE06sol+SOC and PBEsol+$U$+SOC ($0 \leq U \leq 7$ eV) considering spin–orbit coupling (SOC) and non-collinear magnetism. The structural, magnetic and electronic properties were investigated for nine magnetic orders: ferromagnetic <100>, <110> and <111>; longitudinal antiferromagnetic 1k, 2k and 3k; and transverse antiferromagnetic 1k, 2k and 3k magnetic orders.

Our data suggests that only a very small difference exists between FM and AFM magnetic orders, and that they may coexist. Using HSE06sol+SOC, we found FM <110> and FM <111> orders to be the most stable for $PuH_2$ and $PuH_3$, respectively. Using PBEsol+$U$+SOC, the order of stability is dependent on the value of the Hubbard parameter $U$, with a transition from AFM to FM seen in $PuH_2$ at $U$ = 5 eV, whilst an FM to AFM transition is observed at $U$ = 6 eV in $PuH_3$. Of the nine magnetic orders investigated, we determined that only the L3kAFM order retains the experimentally measured $Fm\bar{3}m$ structure. We determined that both cubic $PuH_2$ and $PuH_3$ have metallic behaviour using PBEsol+$U$+SOC ($U$ = 5 eV).

**Supplementary Materials:** The following supporting information can be downloaded at: https://www.mdpi.com/article/10.3390/cryst12101499/s1. The SI contains three sections, organised as follows: Section S1: Convergence testing of cubic $PuH_2$ and $PuH_3$ using PBEsol+$U$+SOC. Section S2: Energetics and structural properties of cubic $PuH_2$ and $PuH_3$ calculated with PBEsol+$U$+SOC+D3; Section S3: Magnetic, structural and electronic properties of cubic $PuH_2$ and $PuH_3$. References [29,42,49] are cited in the Supplementary Materials.

**Author Contributions:** T.S., S.M. and M.M. performed the calculations and data analysis. D.J.C., L.J.G. and E.L.d.S. provided support and discussion. R.M.H. and M.T.S. provided comment on the comparison with experiments. M.M. and T.S. devised the research project. All authors have read and agreed to the published version of the manuscript.

**Funding:** We would like to acknowledge the EPSRC DTP 2018-19 University of Huddersfield (EP/R513234/1). Analysis was performed on the Orion computing facility at the University of Huddersfield. Calculations were run on the ARCHER and ARCHER2 UK National Supercomputing Services via our membership of the UK HEC Materials Chemistry Consortium (MCC; EPSRC EP/L000202, EP/R029431). EldS acknowledges the Network of Extreme Conditions Laboratories (NECL), financed by FCT and co-financed by NORTE 2020, through the programme Portugal 2020 and FEDER. To the extent that this paper relies on the contribution of RMH/MTS, then the copyright vests in the @British Crown Copyright 2020/AWE.

**Institutional Review Board Statement:** Not Applicable.

**Informed Consent Statement:** Not Applicable.

**Data Availability Statement:** The data presented in this study is available on request from the corresponding author.

**Conflicts of Interest:** The authors declare no conflict of interest.

## References

1. Patterson, W. Fifty years of hopes and fears. *Nature* **2007**, *449*, 664. [CrossRef]
2. Hyatt, N.C. Safe management of the UK separated plutonium inventory: A challenge of materials degradation. *NPJ Mater. Degrad.* **2020**, *4*, 1. [CrossRef]
3. Nuclear Decommissioning Authority. *Progress on Plutonium Consolidation, Storage and Disposition*; Nuclear Decommissioning Authority: Moor Row, UK, 2019.
4. Oetting, F.L. The Chemical Thermodynamic Properties of Plutonium Compounds. *Chem. Rev.* **1967**, *67*, 261. [CrossRef]
5. Haschke, J.M.; Hodges, A.E.; Lucas, R.L. Equilibrium and structural properties of the PuH system. *J. Less-Common Met.* **1987**, *133*, 155. [CrossRef]
6. Allen, T.H.; Haschke, J.M. *Hydride-Catalyzed Corrosion of Plutonium by Air: Initiation by Plutonium Monoxide Monohydride*; LA-13462-MS; Los Alamos National Lab.: Los Alamos, NM, USA, 1998. [CrossRef]

7. Haschke, J.M.; Allen, T.H. Plutonium hydride, sesquioxide and monoxide monohydride: Pyrophoricity and catalysis of plutonium corrosion. *J. Alloys Compd.* **2001**, *320*, 58. [CrossRef]
8. Hecker, S.S.; Martz, J.C. Plutonium Aging: From Mystery to Enigma. In *Ageing Studies and Lifetime Extension of Materials*; Springer: Boston, MA, USA, 2001; pp. 23–52.
9. Ganda, F.; Greenspan, E. Incineration of Plutonium in PWR Using Hydride Fuel. In Proceedings of the 2005 International Conference on Advances in Nuclear Power Plants, ARWIF-2005, Oak Ridge, TN, USA, 6–18 February 2005.
10. Ganda, F.; Greenspan, E. Plutonium recycling in hydride fueled PWR cores. *Nucl. Eng. Des.* **2009**, *239*, 1489. [CrossRef]
11. Wicke, O.J. (Ed.) *Plutonium Handbook: A Guide to the Technology*; American Nuclear Society: La Grange Park, IL, USA, 1992.
12. Flotow, H.E.; Haschke, J.M.; Yamauchi, S. Part 9—The Actinide Hydrides. In *The Chemical Thermodynamics of Actinide Elements and Compounds*; IAEA: Vienna, Austria, 1984; p. 115.
13. Haschke, J.M.; Stakebake, J.L. Handling, Storage, and Disposition of Plutonium and Uranium. In *The Chemistry of the Actinide and Transactinide Elements*; Springer: Dordrecht, The Netherlands, 2007; pp. 3199–3272.
14. Stakebake, J.L. The storage behavior of plutonium metal, alloys, and oxide: A review. *J. Nucl. Mater.* **1971**, *38*, 241. [CrossRef]
15. Hecker, S.S. Plutonium—An element never at equilibrium. *Metall. Mater. Trans. A Phys. Metall. Mater. Sci.* **2008**, *39*, 1585. [CrossRef]
16. Ai, J.; Liu, T.; Gao, T.; Ao, B. First-principles study of electronic structure and metal-insulator transition of plutonium dihydride and trihydride. *Comput. Mater. Sci.* **2012**, *51*, 127. [CrossRef]
17. Ao, B.Y.; Wang, X.L.; Shi, P.; Chen, P.H.; Ye, X.Q.; Lai, X.C.; Gao, T. First-principles LDA + U calculations investigating the lattice contraction of face-centered cubic Pu hydrides. *J. Nucl. Mater.* **2012**, *424*, 183. [CrossRef]
18. Li, S.; Ao, B.; Ye, X.; Qiu, R.; Gao, T. New Insights into the Crystal Structures of Plutonium Hydrides from First-Principles Calculations. *J. Phys. Chem. C* **2018**, *122*, 10103. [CrossRef]
19. Ao, B.Y.; Ai, J.J.; Gao, T.; Wang, X.L.; Shi, P.; Chen, P.H.; Ye, X.Q. Metal-insulator transition of plutonium hydrides: DFT + U calculations in the FPLAPW basis. *Chin. Phys. Lett.* **2012**, *29*, 017102. [CrossRef]
20. Ao, B.Y.; Shi, P.; Guo, Y.; Gao, T. The abnormal lattice contraction of plutonium hydrides studied by first-principles calculations. *Chin. Phys. B* **2013**, *22*, 037103. [CrossRef]
21. Guo, Y.; Ai, J.J.; Gao, T.; Ao, B.Y. Structural, magnetic, electronic, and elastic properties of face-centered cubic PuHx (x = 2, 3): GGA (LSDA) + U + so. *Chin. Phys. B* **2013**, *22*, 057103. [CrossRef]
22. Sudhapriyanga, G.; Santhosh, M.; Rajeswarapalanichamy, R.; Iyakutti, K. First Principles Study of Pressure Induced Phase Transition, Electronic and magnetic Properties of Plutonium trihydride. *Int. J. Sci. Eng. Res.* **2014**, *5*, 114.
23. Zhang, C.; Yang, Y.; Zhang, P. Thermodynamics Study of Dehydriding Reaction on the $PuO_2$(110) Surface from First Principles. *J. Phys. Chem. C* **2018**, *122*, 7790. [CrossRef]
24. Yang, Y.; Zhang, P. Hydriding and dehydriding energies of PuHx from ab initio calculations. *Phys. Lett. A* **2015**, *379*, 1649. [CrossRef]
25. Zheng, J.J.; Li, W.D.; Li, S.N.; Zhang, P.; Wang, B.T. Mechanical and thermodynamic properties of plutonium dihydride. *J. Alloys Compd.* **2018**, *750*, 258. [CrossRef]
26. Zheng, J.J.; Wang, B.T.; Di Marco, I.; Li, W.D. Electronic structure and phase stability of plutonium hydrides: Role of Coulomb repulsion and spin-orbital coupling. *Int. J. Hydrogen Energy* **2014**, *39*, 13255. [CrossRef]
27. Li, R.S.; Lu, X.; Wang, J.T.; Xin, D.Q.; Yao, X.G. A many-body perspective on dual 5f states in two plutonium hydrides. *Chem. Phys. Lett.* **2020**, *740*, 137079. [CrossRef]
28. Li, S.; Guo, Y.; Ye, X.; Gao, T.; Ao, B. Structural, magnetic, and dynamic properties of $PuH_{2+x}$ (x = 0, 0.25, 0.5, 0.75, 1): A hybrid density functional study. *Int. J. Hydrogen Energy* **2017**, *42*, 30727–30737. [CrossRef]
29. Muromura, T.; Yahata, T.; Ouchi, K.; Iseki, M. The variation of lattice parameter with hydrogen content of non-stoichiometric plutonium dihydride. *J. Inorg. Nucl. Chem.* **1972**, *34*, 171. [CrossRef]
30. Willis, J.O.; Ward, J.W.; Smith, J.L.; Kosiewicz, S.T.; Haschke, J.M.; Hodges, A.E. Electronic properties and structure of the plutonium-hydrogen system. *Phys. B C* **1985**, *130*, 527. [CrossRef]
31. Kresse, G.; Furthmüller, J. Efficient iterative schemes for ab initio total-energy calculations using a plane-wave basis set. *Phys. Rev. B* **1996**, *54*, 11169. [CrossRef] [PubMed]
32. Heyd, J.; Scuseria, G.E.; Ernzerhof, M. Hybrid functionals based on a screened Coulomb potential. *J. Chem. Phys.* **2003**, *118*, 8207. [CrossRef]
33. Steiner, S.; Khmelevskyi, S.; Marsmann, M.; Kresse, G. Calculation of the magnetic anisotropy with projected-augmented-wave methodology and the case study of disordered Fe1-xCox alloys. *Phys. Rev. B* **2016**, *93*, 224425. [CrossRef]
34. Csonka, G.I.; Perdew, J.P.; Ruzsinszky, A.; Philipsen, P.H.T.; Lebègue, S.; Paier, J.; Vydrov, O.A.; Ángyán, J.G. Assessing the performance of recent density functionals for bulk solids. *Phys. Rev. B* **2009**, *79*, 155107. [CrossRef]
35. Schimka, L.; Harl, J.; Kresse, G. Improved hybrid functional for solids: The HSEsol functional. *J. Chem. Phys.* **2011**, *134*, 024116. [CrossRef]
36. Liechtenstein, A.I.; Anisimov, V.I.; Zaanen, J. Density-functional theory and strong interactions: Orbital ordering in Mott-Hubbard insulators. *Phys. Rev. B* **1995**, *52*, R5467. [CrossRef]
37. Dudarev, S.; Botton, G. Electron-energy-loss spectra and the structural stability of nickel oxide: An LSDA + U study. *Phys. Rev. B* **1998**, *57*, 1505. [CrossRef]

38. Moxon, S.; Symington, A.R.; Tse, J.S.; Dawson, J.; Flitcroft, J.M.; Parker, S.C.; Cooke, D.J.; Harker, R.M.; Molinari, M. The energetics of carbonated $PuO_2$ surfaces affects nanoparticle morphology: A DFT+: U study. *Phys. Chem. Chem. Phys.* **2020**, *22*, 7728. [CrossRef] [PubMed]
39. Pegg, J.T.; Shields, A.E.; Storr, M.T.; Wills, A.S.; Scanlon, D.O.; de Leeuw, N.H. Hidden magnetic order in plutonium dioxide nuclear fuel. *Phys. Chem. Chem. Phys.* **2018**, *20*, 20943. [CrossRef] [PubMed]
40. Pegg, J.T.; Aparicio-Anglès, X.; Storr, M.; de Leeuw, N.H. DFT + U study of the structures and properties of the actinide dioxides. *J. Nucl. Mater.* **2017**, *492*, 269. [CrossRef]
41. Desgranges, L.; Ma, Y.; Garcia, P.; Baldinozzi, G.; Siméone, D.; Fischer, H.E. What Is the Actual Local Crystalline Structure of Uranium Dioxide, $UO_2$? A New Perspective for the Most Used Nuclear Fuel. *Inorg. Chem.* **2017**, *56*, 321. [CrossRef] [PubMed]
42. Grimme, S.; Antony, J.; Ehrlich, S.; Krieg, H. A consistent and accurate ab initio parametrization of density functional dispersion correction (DFT-D) for the 94 elements H-Pu. *J. Chem. Phys.* **2010**, *132*, 154104. [CrossRef]
43. Aldred, A.T.; Cinader, G.; Lam, D.J.; Weber, L.W. Magnetic properties of neptunium and plutonium hydrides. *Phys. Rev. B* **1979**, *19*, 300. [CrossRef]
44. Kim, J.W.; Mun, E.D.; Baiardo, J.P.; Smith, A.I.; Richmond, S.; Mitchell, J.; Schwartz, D.; Zapf, V.S.; Mielke, C.H. Detecting low concentrations of plutonium hydride with magnetization measurements. *J. Appl. Phys.* **2015**, *117*, 053905. [CrossRef]
45. Cinader, G.; Zamir, D.; Hadari, Z. NMR study of the plutonium hydride system. *Phys. Rev. B* **1976**, *14*, 912. [CrossRef]
46. Yang, X.; Yang, Y.; Lu, Y.; Sun, Z.; Hussain, S.; Zhang, P. First-principles GGA + U calculation investigating the hydriding and diffusion properties of hydrogen in $PuH_{2+x}$, $0 \leq x \leq 1$. *Int. J. Hydrogen Energy* **2018**, *43*, 13632. [CrossRef]
47. Dorado, B.; Amadon, B.; Freyss, M.; Bertolus, M. DFT + U calculations of the ground state and metastable states of uranium dioxide. *Phys. Rev. B* **2009**, *79*, 235125. [CrossRef]
48. Meredig, B.; Thompson, A.; Hansen, H.A.; Wolverton, C.; Van De Walle, A. Method for locating low-energy solutions within DFT + U. *Phys. Rev. B* **2010**, *82*, 195128. [CrossRef]
49. Mulford, R.N.R.; Sturdy, G.E. The Plutonium-Hydrogen System. I. Plutonium Dihydride and Dideuteride. *J. Am. Chem. Soc.* **1955**, *77*, 3449. [CrossRef]
50. Mulford, R.N.R.; Sturdy, G.E. The Plutonium-Hydrogen System. II. Solid Solution of Hydrogen in Plutonium Dihydride. *J. Am. Chem. Soc.* **1956**, *78*, 3897. [CrossRef]
51. Ward, J.W. Electronic structure and bonding in transuranics: Comparison with lanthanides. *J. Less-Common Met.* **1983**, *93*, 279. [CrossRef]
52. Haschke, J.M.; Hodges, A.E.; Smith, C.M.; Oetting, F.L. Equilibria and thermodynamic properties of the plutonium-hydrogen system. *J. Less-Common Met.* **1980**, *73*, 41. [CrossRef]